Journal of Applied Physics

RESEARCH ARTICLE | JANUARY 29 2024

Observation of the local electromechanical response in 2–2 ceramic–ceramic lead-free ferroelectric composites via digital image correlation

Alexander Martin ; Juliana G. Maier ; Ken-ichi Kakimoto ; Marc Kamlah ; Kyle G. Webber

J. Appl. Phys. 135, 044102 (2024)
https://doi.org/10.1063/5.0184763

Journal of Applied Physics ARTICLE pubs.aip.org/aip/jap

Observation of the local electromechanical response in 2–2 ceramic–ceramic lead-free ferroelectric composites via digital image correlation

Cite as: J. Appl. Phys. **135**, 044102 (2024); doi: 10.1063/5.0184763
Submitted: 26 October 2023 · Accepted: 8 January 2024 ·
Published Online: 29 January 2024

Alexander Martin,[1,2,a)] Juliana G. Maier,[2] Ken-ichi Kakimoto,[1] Marc Kamlah,[3] and Kyle G. Webber[2]

AFFILIATIONS

[1]Department of Life Science and Applied Chemistry, Graduate School of Engineering, Nagoya Institute of Technology, Nagoya, Japan
[2]Department of Materials Science and Engineering, Friedrich-Alexander-Universität Erlangen-Nürnberg (FAU), Erlangen, Germany
[3]Institute for Applied Materials (IAM), Karlsruhe Institute of Technology, Eggenstein-Leopoldshafen, Germany

[a)]**Author to whom correspondence should be addressed:** martin.alexander@nitech.ac.jp

ABSTRACT

This study investigates bilayers of $0.94(Na_{1/2}Bi_{1/2})TiO_3$–$0.06BaTiO_3$ (NBT–6BT) and $0.90(Na_{1/2}Bi_{1/2})TiO_3$–$0.06BaTiO_3$–$0.04(K_{0.5}Na_{0.5})NbO_3$ (NBT–6BT–4KNN) using digital image correlation, enabling the separate analysis of strain response in each layer. The bilayers were electrically connected without mechanical connection (polarization coupled) as well as mechanically and electrically connected (polarization and strain coupled) to determine the role of interlayer mechanical interactions. The large signal longitudinal and transverse piezoelectric coefficients, d^*_{33} and d^*_{31}, were characterized for both cases. In the polarization coupled composite, d^*_{33} decreased linearly from 410 to 260 pm/V with increasing vol. % NBT–6BT. In contrast, in the polarization and strain coupled case, d^*_{33} and d^*_{31} were maximum at 50 vol. % NBT–6BT with values of 440 and −130 pm/V, respectively, highlighting the critical role of strain interactions in ceramic–ceramic composites. The stress-induced phase transformation through strain coupling significantly impacted the electromechanical response, with improved strain values observed in the NBT–6BT–4KNN layer. Furthermore, this study highlights the variability in the significance of strain coupling within bilayer systems as a function of the altering volume fraction of their constituent components.

I. INTRODUCTION

Actuators based on the piezoelectric effect offer numerous advantages, including high response speeds, displacement accuracy, force generation, low power consumption, and low noise levels.[1] Consequently, they find applications in various fields, such as fuel injection, positioning devices, etc.[1,2] In these applications, the electromechanical strain plays a pivotal role, making it a deciding factor in selecting a suitable material. Currently, ferroelectric materials based on lead titanate zirconate [$(Pb,Zr)TiO_3$, PZT],[2] sodium potassium niobate [$(Na,K)NbO_3$, NKN],[3] barium titanate ($BaTiO_3$, BT),[3] and sodium bismuth titanate [$(Na_{1/2}Bi_{1/2})TiO_3$, NBT][1,4–6] are potential candidates. Due to environmental concerns,[1,2] lead-free materials receive special consideration. Here, NBT-based systems are especially attractive for actuator applications due to their large signal longitudinal piezoelectric strain coefficient d^*_{33} (Refs. 4–6) and high resistance against electrical fatigue.[7] Electric field-induced strains of up to 0.74% at an electric field of 7 kV/mm have been observed, resulting in a d^*_{33} of approximately 1057 pm/V.[5] For comparison, soft PZT (PIC151) reaches strains of approximately 0.3% at an electric field of 6 kV/mm ($d^*_{33} \sim 500$ pm/V).[4] At similar electric fields of 4 kV/mm, NBT-based systems show a larger d^*_{33} of approximately 1263 pm/V[5] compared to commercial PZT ($d^*_{33} \sim 575$ pm/V).[6] However, achieving these large strains in NBT materials requires relatively large electric fields (>2 kV/mm)[4,5] and corresponding large hysteretic behavior, which can result in self-heating and eventual component degradation. Therefore, a major goal of optimizing

NBT-based materials is reducing the driving field while maintaining a large strain.

NBT exhibits a perovskite crystal structure that has been extensively investigated over several studies.[8–14] Previous research has provided evidence supporting a monoclinic (Cc)[8,9] crystal phase and a rhombohedral phase ($R3c$)[10,11] in NBT at room temperature. Additionally, more complex systems, such as a mixed phase comprising both Cc and $R3c$ phases,[12] as well as the presence of tetragonal ($P4bm$) platelets within a rhombohedral matrix,[13,14] have been proposed. The intricate nature of the crystal structure can be attributed to the chemical heterogeneity caused by the Na/Bi positional disorder.[15] Furthermore, NBT exhibits relaxor-like characteristics and, similar to ferroelectric materials, displays piezoelectric properties after poling with a d_{33} ranging between 73 and 95 pC/N at room temperature.[16,17] To improve the electromechanical properties, NBT is generally combined with other perovskite materials, such as $Bi_{1/2}K_{1/2}TiO_3$,[18,19] $SrTiO_3$,[20,21] and BT.[22–26] In particular, solid solutions of $(1-x)(Na_{1/2}Bi_{1/2})TiO_3$–$xBaTiO_3$ (NBT–100xBT) have garnered particular interest due to the observed morphotropic phase boundary (MPB) at a BT-content of approximately 6–7 mol. %,[22–24] with maximized electromechanical properties ($d_{33} \sim 150$ pC/N).[24,25] Relaxor ferroelectrics, such as NBT–BT compositions, depolarize at the ferroelectric-to-relaxor phase transition temperature (T_{F-R}) that separates the electric field-induced long-range ferroelectric order from the higher temperature ergodic relaxor state. For instance, the T_{F-R} of NBT–6BT is found at approximately 83 °C.[25] Below this temperature, NBT–6BT is classified as a nonergodic relaxor,[6,27] meaning that under the influence of an electric field, the material undergoes an irreversible phase transformation to a long-range ferroelectric order.[23,24] Similar observations have also been documented in lead-containing relaxors, such as $Pb_{1-x}La_x(Zr_yTi_{1-y})_{1-x/4}TiO_3$ (PLZT)[28,29] and $Pb(Mg_{1/3}Nb_{2/3})O_3$ (PMN).[30] It should be noted that the ferroelectric phase can also be stabilized via mechanical stress.[31] Above T_{F-R}, a reversible electric field-induced long-range ferroelectric order is observed, and the material is referred to as ergodic relaxor (ER). Because of the reversibility of the electric-field-induced state change, a loss of remanent polarization and strain is observed, increasing the usable unipolar strain response.[6,32] The nonergodic relaxor behavior can also be chemically destabilized by shifting the T_{F-R} below room temperature. This can be achieved by using ternary systems, such as $(Na_{1/2}Bi_{1/2})TiO_3$–$BaTiO_3$–$(K_{0.5}Na_{0.5})NbO_3$ (NBT–BT–KNN).[4] For that reason, NBT–BT–KNN compositions show a high strain of 0.45% at electric fields of 8 kV/mm. However, as mentioned previously, relatively large polarization fields (>2 kV/mm) are required,[4,5] which reduces the usability of these materials in engineered structures.

One approach to reducing the required electric field for inducing the large strain response is to utilize ceramic–ceramic composites, which involve combining two suitable ceramic materials.[33] The suitability of the constituents depends on their dielectric properties, which play an important role in determining the internal electric field distribution.[33–35] Here, previous studies have presented a simple series capacitor model to explain the effect of polarization coupling.[33–35] Assuming a stress-free state with ideal capacitors, i.e., infinite resistance, the charge in both capacitors is coupled, whereas the voltage distribution and, therefore, the local electric field on each capacitor are based on the capacitance and polarizability of the material.[34,35] Dausch *et al.* have employed this concept on lead-based ferroelectric (FE) and antiferroelectric (AFE) 0–3 type composites.[36,37] In these composites, ferroelectric particles, acting as seeds, were distributed within an AFE material, serving as the matrix. As a result, a reduction of the required electric field for the phase transformation from AFE to FE was observed. Lee *et al.* demonstrated similar behavior in ER–FE composites using $(1-x)Bi_{1/2}(Na_{0.75}K_{0.25})_{1/2}TiO_3$–$xBiAlO_3$ (BNKT–100xBA) as the ER matrix phase and NBT as the FE seed phase.[34] With the inclusion of NBT, the necessary electric field to induce the phase transformation was effectively reduced, and large d^*_{33} values of 725 and 548 pm/V were achieved for BNKT–7BA with 20 vol. % NBT and BNKT–6BA with 10 vol. % NBT, respectively.[34] Similar results were observed by Groh *et al.* in the system $0.92Na_{1/2}Bi_{1/2}TiO_3$–$0.06BaTiO_3$–$0.02K_{0.5}Na_{0.5}NbO_3$ (NBT–6BT–2KNN) and NBT–7BT, with NBT–6BT–2KNN as the ER matrix phase and NBT–7BT as the FE seed phase.[38,39] Despite these promising results, the underlying mechanisms are not fully understood, as factors, such as interdiffusion between the constituents, strain coupling, etc., contribute to the overall electromechanical response. As such, studies focused on different contributions of different material systems.[40–45] For instance, Fan *et al.* used finite element simulation to determine the electric field distribution in $0.75(Na_{1/2}Bi_{1/2})TiO_3$–$0.25SrTiO_3$ (ER) and $0.96Bi_{1/2}(Na_{0.84}K_{0.16})_{1/2}TiO_3$–$0.04SrTiO_3$ (FE) 3-0 composites.[40] Here, the internal electric field within the ER phase surpassed the applied field, while within the FE phase, the opposite case was observed.[40] Furthermore, Saleem *et al.* focused on the interdiffusion aspect by using different sintering times during the production of the composites with $0.74(Na_{1/2}Bi_{1/2})TiO_3$–$0.26SrTiO_3$ as the ER matrix phase and $0.9(Na_{1/2}Bi_{1/2})TiO_3$–$0.1SrTiO_3$ as the FE seed phase.[46] It was found that with increasing interdiffusion, the material shifted to more ferroelectric characteristics, effectively decreasing the overall maximum strain,[46] showing the importance of separating the two phases. Another study that focused on the interdiffusion aspect was conducted by Ayrikyan *et al.*[44] Here, the local chemical and residual stresses of trilayer composite structures of NBT–7BT and BNKT–6BA were investigated.[44] They identified that the interdiffusion between the constituents and internal residual stresses led to significant changes in the crystal structure, elastic properties, and grain size, particularly in the NBT–7BT layer.[44] As such, co-sintering of the constituent materials adds a layer of complexity to the overall system. In order to mitigate the intricacies involved, the authors have recently highlighted the importance of mainly strain coupling in 2–2 composites of 0.90NBT–0.06BT–0.04KNN (NBT–6BT–4KNN) and NBT–6BT[45] with end-member volume fractions of 50–50. Instead of co-sintering, the materials were (i) electrically connected and (ii) both mechanically and electrically connected. Thus, via a custom-built digital image correlation (DIC) system, the local strain through the thickness of the composite across different layers could be determined. Due to strain coupling, biaxial stress was applied to the NBT–6BT–4KNN layer, improving the electromechanical properties. As such, the overall large signal piezoelectric coefficient d^*_{33} was enhanced to 440 pm/V due to strain coupling for the case of 50 vol. % compared to the end-member material NBT–6BT–4KNN ($d^*_{33} = 390$ pm/V).[45]

However, as shown in previous studies,[38,39] the ratio between the constituent materials also plays a pivotal role. The open

question remains if the influence of strain coupling also depends on the volume fraction of the constituents. For this reason, the current study will focus on how polarization and strain coupling effects change with varying volume fractions. The DIC method was employed to record the complete deformation behavior of each layer and the composite during the electric field loadings. Similar to the previous study,[45] (i) electrically connected and (ii) mechanically and electrically connected bilayer samples will be observed.

II. EXPERIMENTAL METHODOLOGY

NBT–6BT–4KNN and NBT–6BT powders were produced via the solid oxide synthesis route and chosen for matrix and seed material for the bilayer structure, respectively. Starting powders are Na_2CO_3 (99.95% purity, Alfa Aesar), Bi_2O_3 (99.975% purity, Alfa Aasar), TiO_2 (99.6% purity, Alfa Aesar), $BaCO_3$ (99.95% purity, Alfa Aesar) K_2CO_3 (99.95% purity, Alfa Aesar), and Nb_2O_5 (99.95% purity, Alfa Aesar). The two powders were separately uniaxially pressed into disks with an approximate diameter of 7 mm and a thickness of approximately 7 mm and subsequently cold-isostatically pressed at −180 MPa. Afterward, the green bodies were sintered at 1150 °C for 3h using a heating and cooling rate of 3 °C/min. In addition, sacrificial powder of the same compositions was used. Samples were cut and ground into rectangular samples with a surface area of $4.5 \times 4.5\ mm^2$. The relative densities, determined via the Archimedes method, were 96.7% ± 0.3% and 97.2% ± 0.7% for NBT–6BT and NBT–6BT–4KNN. More information about the microstructures can be found in Fig. S1 of the supplementary material. A central aim of this study is the influence of the volume ratio between the matrix (NBT–6BT–4KNN) and the seed (NBT–6BT) material. In order to produce bilayers with different volume ratios, the height of the end members was changed accordingly, whereas the total height of the resulting bilayer sample was kept constant at 4 mm. Bilayers, with a volume ratio between 0% and 100% seed, were measured. The top and bottom surface areas of the sample were sputtered with gold electrodes. After attaching the electrodes, the samples were annealed at 500 °C for 1h with a heating and cooling rate of 5 and 1 °C/min, respectively. This was done to reduce internal stresses and stress-induced ferroelectric phases. Two different cases have been tested with this varying volume ratios. In case (i), the samples were stacked to create an electrical contact; it was assumed that the samples could freely move laterally during electrical loading, and no significant mechanical contact was induced. In case (ii), the samples were additionally mechanically connected with a conducting silver paste, forming a mechanical and electrical connection between the samples. From here, case (i) will be denoted as polarization coupled (PC) and case (ii) as polarization and strain coupled (PSC). For each case and varying volume fractions, three large field electrical measurements were conducted.

In order to measure the electromechanical response of the bilayer samples, a Sawyer–Tower circuit with a reference capacitor $C_{ref} = 4.65\,\mu F$ was used to measure the resulting total electric field-dependent polarization. Additionally, the total strain of the bilayers was measured with a linear variable differential transformer (LVDT). Electric fields with a bipolar triangular waveform, maximum values of ±4 kV/mm, and a loading rate of $0.16\ kV/mm\ s^{-1}$ (0.01 Hz) were applied with a high-voltage power amplifier (30/20 A, TREK, Inc.) and a custom LabVIEW-based waveform generator. One cycle of electric field loading was applied to the samples from the unpoled, virgin state. However, the applied electric fields do not necessarily represent the local electric fields in the materials used in the bilayer system due to local variations in the dielectric response.

Digital image correlation was used to observe the electromechanical response of the different layers directly. For that, the setup has an oil bath with a glass window, allowing for the recording of images of one sample surface during the application of an electric field. A digital camera (MC089MG-SY-UB, Ximea GmbH) with a resolution of 4112×2176 pixels combined with a lens with 2× magnification (MVO-TML Telecentric Measuring Lens, Edmund Optics, Inc.) was used to image the sample surface. Overall, a resolution of $1.75\,\mu m$/pixel could be achieved. In order to have trackable patterns for the DIC calculations, artificial speckles were sprayed onto the observation surfaces by means of an airbrush (AT-Airbrush Pistole Kit, AT-AK-02, Agora-Tec). Two images per second were taken to record the deformation during electric field loading and were subsequently analyzed using a commercially available DIC program, Veddac (Version 6.0, Chemnitzer Werkstoffmechanik GmbH). Measurement points were evenly distributed at a distance of 60 pixels (105 μm) with a reference field of 120×120 pixels ($\sim 210 \times 210\,\mu m^2$). The hair wavelet function was chosen to increase accuracy and minimize the standard deviation between points. Additional information about the setup can be found elsewhere.[45]

III. RESULTS AND DISCUSSION

By combining NBT–6BT–4KNN with various volume ratios of NBT–6BT, distinct changes in the macroscopic field-induced strain were observed. Figures 1(a)–1(n) depict the overall longitudinal (S_3) and transverse strain (S_1) response of the end members [Figs. 1(a), 1(g), 1(h), and 1(n)] as well as of the bilayer samples in PC [Figs. 1(b)–1(f)] and PSC [Figs. 1(i)–1(m)] connectivity. Representative curves from the three measurements have been chosen. The LVDT response for all volume ratios was examined and, where possible, compared with the corresponding calculated strains obtained from the DIC results. Importantly, similar responses were observed between the LVDT and DIC measurements, indicating minimal deviation between the two measurement methods. A possible source for the deviation might result from fluctuations of the light reflection due to silicone oil movement, temporally changing the effective image contrast. To reduce this error, the sample was placed as close to the glass window as feasible to decrease the amount of silicone oil between the sample surface and the camera. Additionally, a low loading frequency was used to prevent turbulent oil motion. Image capture for noise evaluation was conducted for 100 s, during which no electric field was applied, and identical DIC parameters were maintained. The recorded background noise registered at 0.04 pixels, approximately equivalent to 0.002% strain.

Figures 1(a), 1(g), 1(h), and 1(n) display the overall response of S_3 and S_1 as a function of electric field for the end members NBT–6BT–4KNN (0 vol. %) and NBT–6BT (100 vol. %), corresponding well with previous reports.[22–26,39,47,48] These data show that NBT–6BT–4KNN, an ergodic relaxor at room temperature,[39,47,48] exhibited low remanent strain ($S_R^{ER} = 0.05\%$) and high

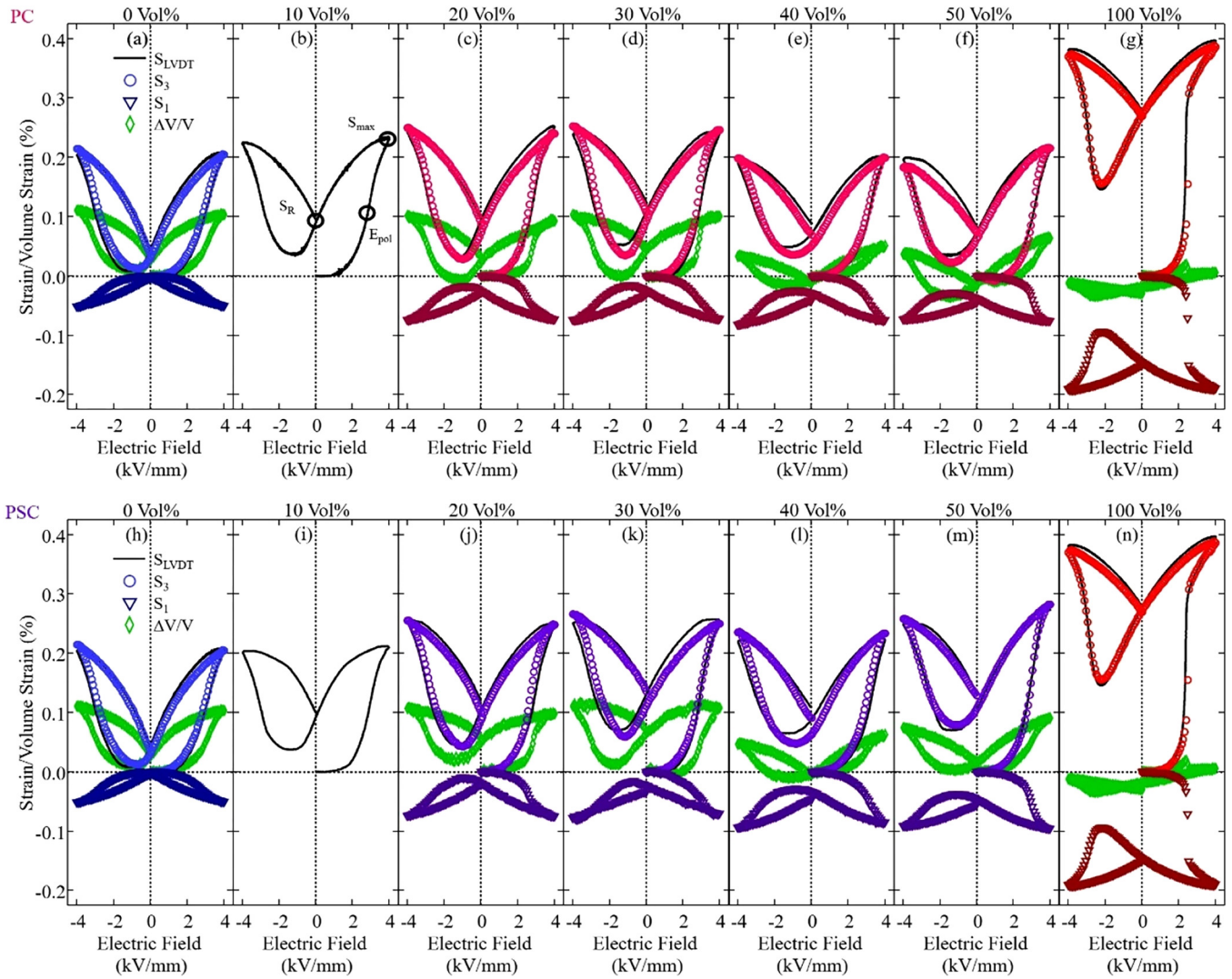

FIG. 1. Longitudinal and transverse strain-electric field hysteresis loops for end-member materials (a), (g), (h), and (n) and PC (b)–(f) and PSC (i)–(m) bilayer samples with varying NBT–6BT contents.

maximum strain ($S^{ER}_{max} = 0.21\%$). On the other hand, NBT–6BT, which in the electrically poled state at room temperature displays long-range ferroelectric order,[22–26] exhibited both, high remanent ($S^{FE}_{R} = 0.25\%$) and maximum strain ($S^{FE}_{max} = 0.36\%$). In addition, the polarization field (E_{pol}), which is the inflection point during the first cycle of applying an electric field and describes the necessary electric field to start coalescence of ferroelectric domains, was observed to be higher for NBT–6BT–4KNN ($E^{ER}_{pol} = 2.7\,\text{kV/mm}$) than for NBT–6BT ($E^{FE}_{pol} = 2.3\,\text{kV/mm}$).

Figures 1(b)–1(f) and 1(i)–1(m) represent the changes to the overall strain response for bilayers with changing vol. %. It should be noted that in the composites with 10 vol. % nonergodic relaxor, only insufficient data points for the DIC measurement could be gathered due to the limited layer thickness (~400 μm) of NBT–6BT; thus, only the LVDT response is presented for these samples. Initially, with an increase in the NBT–6BT content, there is a corresponding increase in both the remanent and maximum strain up to 30 vol. % in both the longitudinal and transverse directions. This is consistent with previous studies, which have shown an increase of the remanent strain with the increase of ferroelectric or nonergodic relaxor seed content.[38–40] However, with further increasing NBT–6BT content for the 2–2 composites at 40 and 50 vol. %, a reduction in the remanent and maximum strain is observed in the PC sample. Interestingly, the 50 vol. % PSC sample displays an increase in both strain values as well as the largest maximum strain from all 2–2 composites. Whereas similar

responses between PC and PSC were observed for the 20 and 30 vol. % samples, larger maximum strains for the PSC samples were achieved for 40 and 50 vol. %. Notably, the samples with 10 vol. % showed a decreased response when mechanically connected. These results show the dependence of the overall response and the influence of strain coupling from the volume fraction of the NBT–6BT layer. In all cases, S_1 closely mirrors the pattern of S_3, albeit with a magnitude approximately a quarter of the longitudinal strain for NBT–6BT–4KNN and half for NBT–6BT.

During the application of an electric field, various phenomena, such as alterations in crystal symmetry, domain configuration, and defect structures, lead to the emergence of localized strains. It is important to highlight that some of these effects conserve the sample volume, such as domain wall motion,[49] while others, such as field-induced structural phase transitions, can result in volume changes.[50] It is worth noting that structural phase transitions induced by an electric field can also arise from deviatoric stress components, as observed in potassium bicarbonate ($KHCO_3$).[51] However, it is recognized that structural transitions are generally interconnected with a change in volume between crystal phases.[50,51] Since the DIC method allows for the evaluation of the longitudinal and transverse strain, it is possible to assess the volume strain ($\Delta V/V$) during electric field loading.[45,52] Assuming an electromechanical response that adheres to transversely isotropic properties, we can determine the volume strain using the following equation:

$$\Delta V/V \cong S_3 + 2S_1. \quad (1)$$

As a result, NBT–6BT, i.e., 100 vol. %, displays negligible volume strain, implying an absence of crystallographic symmetry alterations during the transformation. These findings correspond well with the experimental results from Jo and Rödel,[52] where the volume strain in various NBT–BT compositions was measured for varying BT contents. Conversely, NBT–6BT–4KNN, i.e., 0 vol. %, exhibits a maximum volume expansion of approximately 0.1%, signifying the presence of a field-induced phase transformation.

In the composite case with 20 and 30 vol. %, the maximum volume strain of 0.1% persists in both PSC and PC cases. Furthermore, the remanent volume strain increases compared to the end-member material NBT–6BT–4KNN, which coincides with the increase in S_R^{ER}. The remanent volume strain is maximized at 30 vol. % for both PC and PSC cases, retaining a value of 0.04% and 0.06%, respectively. This increase in volume strain is most likely due to an internal electrical and/or mechanical remanent field across the ER phase. In the PC case, where the layers are not mechanically connected, this remanent field is caused by varying dielectric responses in both phases.[38] In the PSC case, an additional mechanical internal strain field can be introduced due to the differences in electrically induced strain.[41,45] As such, the increased remanent volume and remanent strain in the PSC case, compared to the PC case, could be due to the additional mechanical stress. For instance, transverse compressive stress has been shown to increase the remanent polarization in PZT.[53,54] In addition, Tan *et al.* have shown the opposite effect by revealing a decrease of the remanent polarization with longitudinal uniaxial mechanical stress.[55] Since the ER layer contracts less than the FE layer, the ER layer is under compressive stress, leading to an increased remanent state.[41] Zhang *et al.* have shown that the compressive stress increases with increasing FE layer volume fraction,[41] resulting in a more pronounced effect at elevated volume fractions.

The total polarization as a function of electric field can provide additional information about the domain switching processes. Therefore, the macroscopic polarization-electric field hysteresis behavior for all samples is presented in Figs. 2(a)–2(g). In the case of NBT–6BT–4KNN, a pinched hysteresis characteristic of an ergodic relaxor was observed, resulting in low remanent polarization ($P_R = 15\,\mu C/cm^2$), consistent with previous observations at room temperature.[39,47,48] In contrast, NBT–6BT, a nonergodic relaxor, exhibited no constriction and formed large remanent polarization ($P_R = 43\,\mu C/cm^2$), characteristic for this system.[22–26] Furthermore, NBT–6BT showed higher maximum polarization P_{max} than NBT–6BT–4KNN, which was determined to be 47 and 39 $\mu C/cm^2$, respectively.

In the 2–2 composites, variations in the constituent contents are expected to influence the remanent and maximum polarization values.[35,39] For PC composites, the changes in the polarization response mirror those observed in the macroscopic strain response, namely, the remanent and maximum polarization, increase with higher volume percentages, peaking at 30 vol. % NBT–6BT, followed by a decline at 40 and 50 vol. %. Generally, when two materials are coupled, the charges in each layer remain consistent, unlike the electric field, which can vary depending on the permittivity and volume fraction.[38] In the case of similar thickness and area of two connected materials, the material with higher permittivity experiences a lower electric field and vice versa. This effect can be further magnified with changing volume fraction. Indeed, it was shown that the local electric field of the FE layer is inversely proportional to the layer thickness, meaning that with increasing volume percentages, the local electric field decreased.[38] As such, in composites with 40% and 50% volume fractions, the local electric field is minimized in the FE layer, resulting in significant reductions in both maximum and remanent polarization. Moreover, in the remanent state, a distinct polarity shift occurs—the ER layer experiences a positive remanent field, while the FE layer acquires a negative remanent field.[38] These fields occur in order to maintain an equal charge distribution in both materials. In addition, numerical simulations on NBT–7BT and NBT–6BT–2KNN composites revealed that the smaller the FE volume fraction, the larger the magnitude of the remanent electric field in the FE layer, which is negative in sign.[38] This polarity discrepancy raises the possibility that the negative field within the ferroelectric phase is sufficient to induce depolarization of the ferroelectric layer. Consequently, this depolarization effect plays a pivotal role in diminishing polarization values, particularly concerning remanent polarization.

However, unlike the strain response, the PC and PSC cases did not exhibit significant differences, except at 10 vol. %. Initially, the electric field across the FE layer should be maximized due to minimized layer thickness. However, the discrepancy is likely due to the mechanical constraints on the sample. Zhang *et al.* have demonstrated in a composite system that the FE layer experiences higher tensile stress with lower volume fraction.[41] Whereas transverse compressive stress increases the polarization values,[53,54] transverse tensile stress has the opposite effect. Therefore, when mechanically coupling the materials, NBT–6BT is constrained and

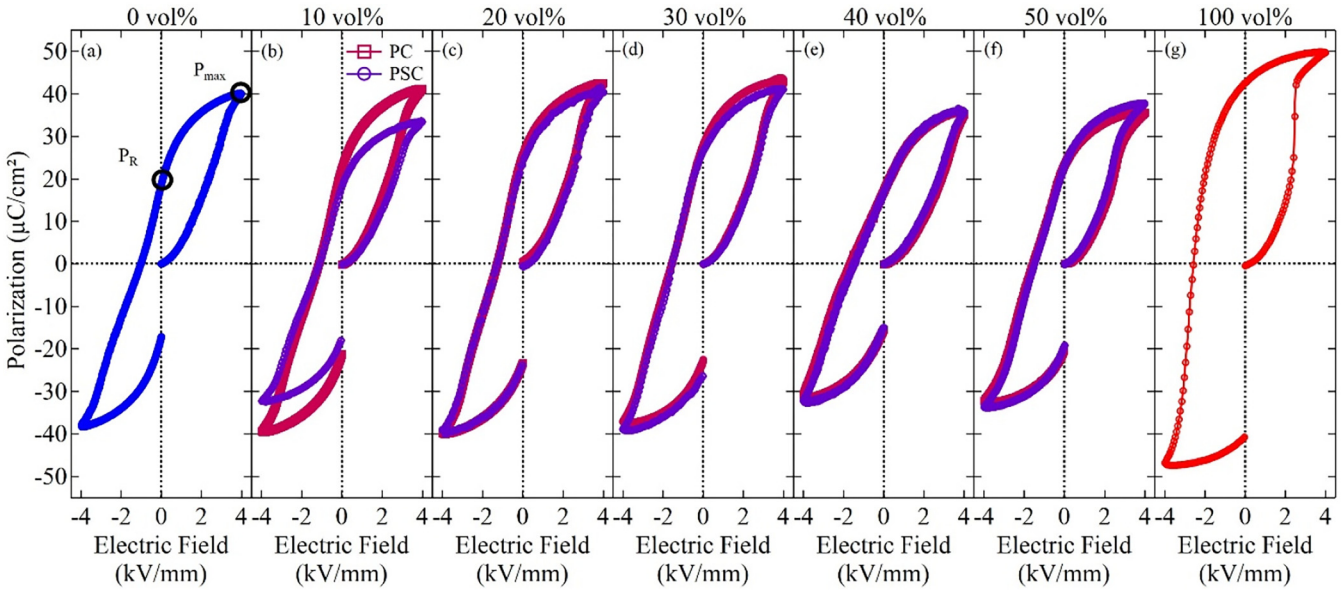

FIG. 2. Electric field-dependent polarization responses for the PC and PSC case with different NBT–6BT volume fractions (b)–(f) as well as the P(E)-hysteresis curves for the end members (a) and (g).

does not fully polarize in the PSC case, resulting in the difference at 10 vol. %.

Considering that the macroscopic strain response for 40 and 50 vol. % changes between the PC and PSC cases, the similarity of the overall P(E)-curves is unexpected. As mentioned earlier, compressive stress on the ER layer increases with the increasing FE layer volume fraction.[41] This coincides well with the growing divergence in the macroscopic strain response between the PC and PSC cases with increasing volume percentages. Dittmer *et al.* have shown for NBT–6BT samples that uniaxial compressive stress changed the electric-field-induced strain more than the polarization response.[56] This decoupling of strain and polarization response was particularly observed around the T_{F-R} where the material shifts to an ergodic relaxor.[56] Nevertheless, measurements of strain and polarization as a function of radial compressive stress would be necessary to resolve this question.

The remanent and maximum strain and polarization values are summarized in Figs. 3(a)–3(f) for the PC and PSC samples as a function of NBT–6BT content. During testing, three different samples were measured for each NBT–6BT content to help observe sample-to-sample variations. For each measurement, the maximum strain was read at the positive and negative electric field and the remanent strain at an electric field of 0. As such, two data points could be extracted for the specific values. In order to improve clarity, the average value is shown in Fig. 3, with the shaded area representing the maximum and minimum observed values. Possible sources for these variations are general sample-to-sample variations, such as differences in microstructure and porosity. However, care was taken to ensure that the observed relative density of each sample via the Archimedes method was >95%. In particular, for the PC case, the quality of the connection between the samples, such as a possible thin layer of oil between the electrodes, is a potential error source. Nevertheless, no significant difference in the size of the error bars between the PC and PSC is visible. Overall, the variations are small enough and allow for a description of the overall trend.

In the PC case up to 30 vol. %, the remanent strain increased, whereas the maximum strain remained relatively constant with increasing NBT–6BT fraction. However, at 40 and 50 vol. %, a local minimum is observed. Generally, as the NBT–6BT content increases, both strain values should, in theory, show an increase according to the rule of mixture. For instance, in previously observed results for 0–3 composites with the same basic materials, Groh *et al.* found a continuous increase of both the remanent and maximum strain with increasing NBT–6BT content. There are different possible explanations for why differences between these results and the current study occurred. For one, the response of 0–3 composites differs from 2–2 composites, as shown by Ayrikyan *et al.*[19] due to differences in the interface regions, interdiffusion, and residual stress state. For example, 0–3 composites have been sintered together, thus producing an interphase between the materials as well as internal stresses caused by varying sintering dynamics. As shown in previous studies, these interphases have crystal structures and electromechanical properties that are different from the bulk, impacting the macroscopic properties.[44] Additionally, in the PC case, the samples are connected only by polarization and not by strain. When focusing on the PSC case, the previously observed local minimum 40 and 50 vol. % in the PC case is less pronounced, and maximum and remanent strain follow a more linear trend.

To further understand the macroscopic strain and polarization results, two important factors will be discussed. First, the applied

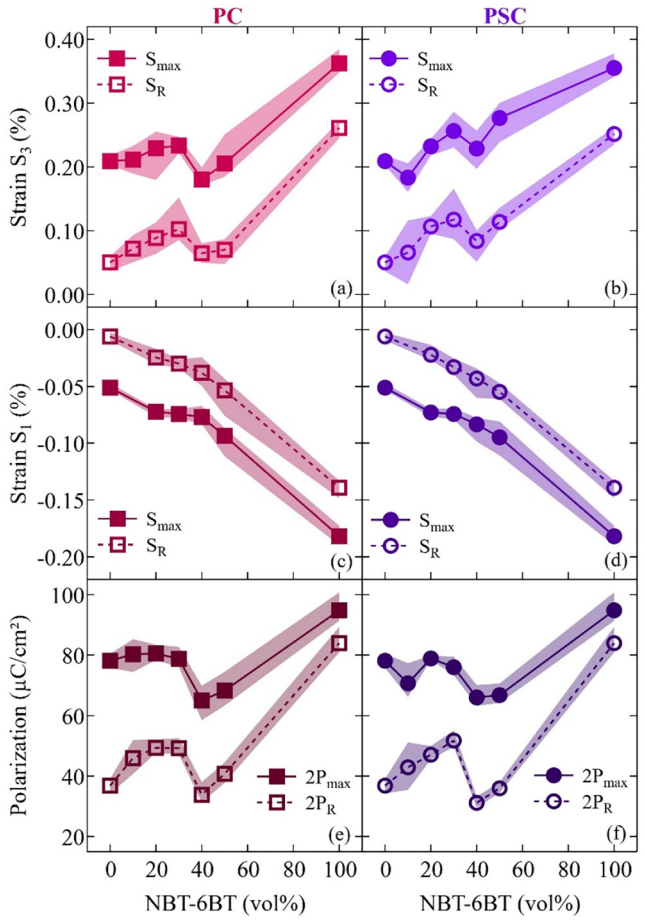

FIG. 3. Overall remanent (S_R) and maximum strain (S_{max}) response for the PC and PSC case at varying NBT–6BT vol. %, as well as the overall remanent ($2P_R$) and maximum polarization ($2P_{max}$). The shaded area represents the maximum and minimum measured values from six data points.

maximum electric field plays an important role. Groh *et al.* directly compared the macroscopic strain response of NBT–6BT–2KNN with 0–3 composites consisting of the NBT–6BT–2KNN matrix and the 10 vol. % NBT–7BT seed at 4 and 6 kV/mm.[38] They found that an enhancement was only observed in the case of 4 kV/mm, whereas in the case of 6 kV/mm, the 10 vol. % sample showed lower achievable large signal piezoelectric properties.[38] Similar observations were made by Zhang *et al.* on the multilayer composite system of $0.91Bi_{1/2}Na_{1/2}TiO_3$–$0.06BaTiO$–$0.03AgNbO_3$ (RE-matrix) and $0.93Bi_{1/2}Na_{1/2}TiO_3$–$0.07BaTiO_3$ (FE-seed).[41] This is due to the saturation of the strain signal at higher electric fields reducing the apparent d^*_{33} coefficient. With increasing seed concentration and subsequent reduction in the polarization field, the composite displays enhanced strain saturation at the same maximum electric field, resulting in an apparent decrease of the large signal piezoelectric coefficient. As such, the applied electric field plays another important role at which vol. % an enhancement is observed. Second, the connectivity of the multilayer structure is important.[41] Here, a previous study reduced the polarization coupling through variations in the electric field orientation with respect to the layer interfaces in 2–2 composites, where layers were connected in parallel (polarization and strain coupled) and perpendicular (strain coupled) to the electrode. Here, the optimum amount of seed was different depending on whether the samples were polarization coupled (25 vol. %, $d^*_{33} \sim 625$ pm/V) or strain coupled (38.2 vol. %, $d^*_{33} \sim 564$ pm/V).[41]

So far, the discussion has been limited to the overall response, but the DIC method allows the observation of individual layers to understand the local strain response [Figs. 4(a)–4(j)]. Furthermore, observations of each layer separately allow for qualitative evaluation of the local electric field in each layer. For the PC case, the assumption is that the polarization fields of the end members do not change in the composite structure. Since polarization fields can be estimated from the strain responses, variations in the evaluated polarization field are caused by variations in the local electric field in each layer. For example, if the polarization field surpasses that of the end members, it is suggested that the local electric field is lower than the applied electric field. These variations in the local electric field arise from the series connection of both layers. When capacitors are connected in series, assuming infinite resistivity, the charge must be equal for both capacitors. In a system with varying dielectric permittivity between components and volume ratio variations between the layers, there is an inhomogeneous distribution of electric field due to different local voltage drops on each capacitor. Additionally, since nonergodic and ergodic relaxors are nonlinear dielectrics, additional information is necessary to evaluate the charge distribution correctly.[57] This is, unfortunately, out of the scope of this research. Nevertheless, varying local electric fields in the NBT–6BT and NBT–6BT–4KNN layers are expected and need to be considered in conjunction with the independent results of the respective end members. For the PSC case, the additional mechanical stresses caused by a strain-mismatch will change the strain response of the layers and, by extension, the polarization field.

In the NBT–6BT layer, the polarization field shifts to higher values with increasing volume fraction, suggesting a decrease in the local electric field in the NBT–6BT layer [Figs. 4(a)–4(e)]. This is further supported by the lower maximum and remanent strain values compared to the end members. As mentioned previously, due to the coupled charge between the FE and ER layers, a remanent field is observed in each layer.[38] Furthermore, the smaller the FE volume fraction, the larger the magnitude of the remanent electric field in the FE phase, which is negative in sign.[38] These observations are particularly prominent in the PC case at 40 and 50 vol. %. At these volume fractions, the most significant difference between PC and PSC cases is visible as well. Compared to the PC case, increased strain values and lower polarization fields are observed for the NBT–6BT layer in the PSC connection. Previous studies have highlighted the crucial role of the strain coupling effect in the reduction of the transformation field.[40,41,45] Due to mechanical coupling, the NBT–6BT layer experiences mechanical stress that facilitates the field-induced transformation into the ferroelectric phase.[28–30] When comparing the electromechanical response, NBT–6BT–4KNN strains at electric fields

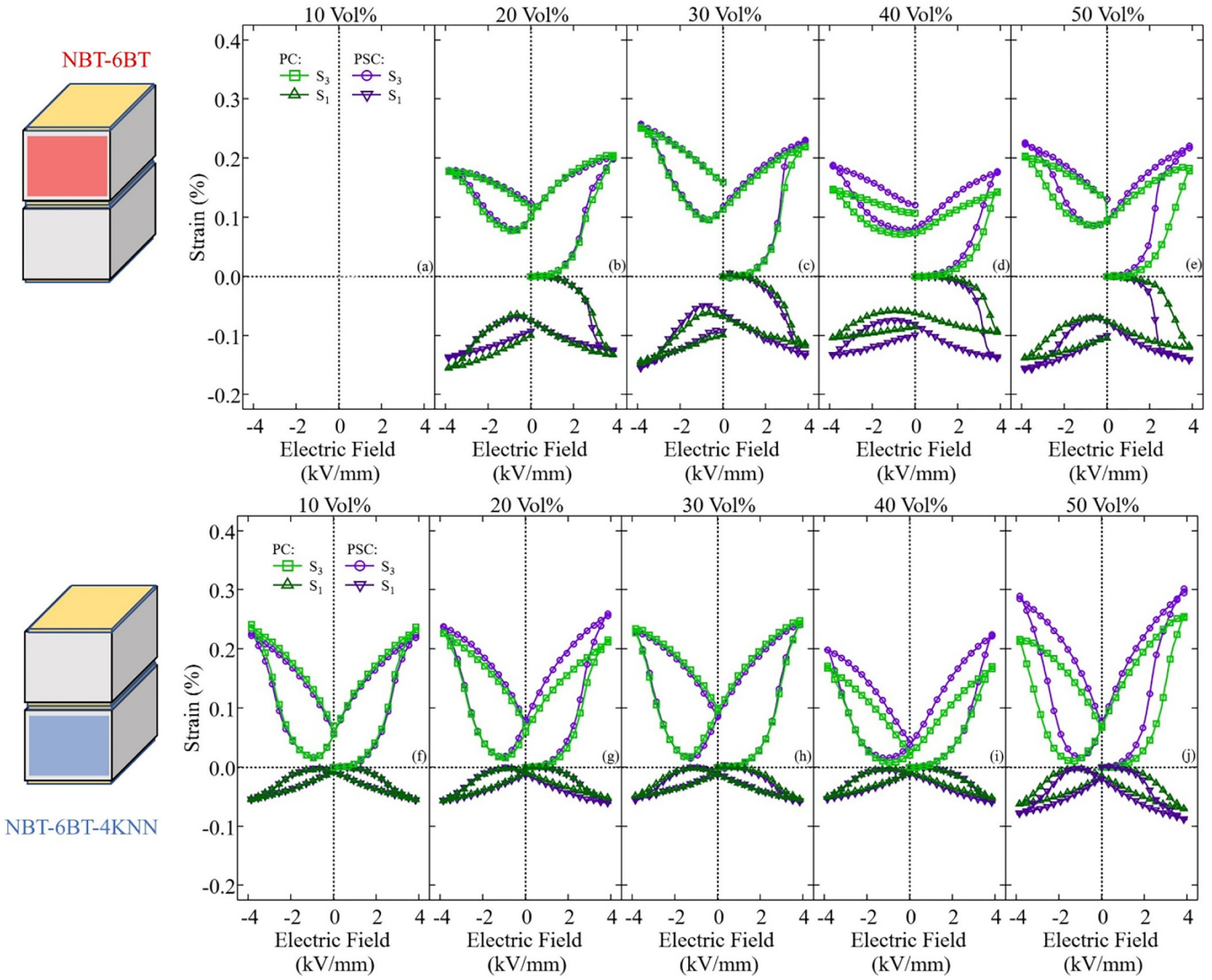

FIG. 4. Local longitudinal and transverse strain-electric field hysteresis loops for the NBT–6BT (a)–(e) and NBT–6BT–4KNN (f)–(j) layers in 2–2 composites with varying NBT–6BT volume fractions.

below the polarization field of NBT–6BT. As such, the ER layer contracts before the FE layer, resulting in a biaxial tensile and compressive stress in the ER and FE layer, respectively. This mechanical stress likely facilitates the phase transformation in NBT–6BT. Furthermore, transversal compressive biaxial stress has been shown to decrease the polarization field in ferroelectric materials.[31,32] This would explain why the polarization field for the NBT–6BT layer is reduced at 40 and 50 vol. %.

Similarly, the strain response of the NBT–6BT–4KNN layer can reveal changes to the local electric field of the ER layer. Figures 4(f)–4(j) show representative S(E)-loops as a function of seed content for NBT–6BT–4KNN. In the PC case, both remanent and maximum strain showed a significant increase with the rise in volume percentage up to 30%. This increase in remanent strain is particularly noteworthy since NBT–6BT–4KNN is typically characterized by a low remanent strain that is nearly independent of the applied electric field.[39,47,48] Mirroring the behavior of the FE layer, the ER layer exhibits an internal remanent electric field caused by the charge equalization between the layers. To counteract the negative field in the FE layer, the internal remanent field in the ER layer is positive, leading to a positive remanent strain.[38] Residual mechanical fields can influence the remanent state as well.[41] Despite the substantial transverse remanent strain in the NBT–6BT end members, they are not expected to play a significant role. This is evident since similar remanent strains are observed in both PC and PSC samples despite the absence of

mechanical coupling in the PC state. However, mechanical fields seem to have played a major role in the enhancement of the strain response at 40 and 50 vol. %. At first, in the PC case, the S (E)-loops of 40 and 50 vol. % appear broader, indicating a higher polarization field and, by extension, a lower local electric field. However, similar to the NBT–6BT layer, the polarization field was reduced in the PSC case compared to the PC case. These results highlight the importance of strain coupling at higher vol. %, particularly in the PSC case for 50 vol. %, where the highest maximum strain of NBT–6BT–4KNN was achieved.

Initially, the PSC and the PC composite are electrically unpoled with zero internal residual stresses. However, in the PSC case, upon the application and subsequent removal of an external electric field, the transverse electromechanical response alters the internal stress within the composite. To illustrate this point, Figs. 5(a) and 5(b) depict the electric-field-induced strain response of the sample with 40 vol. % NBT–6BT. Since DIC allows for the local resolution of the strain response, four points have been selected. Two points were selected from a sufficient distance (~500 μm) to the interface, where the strain describes bulk strain behavior of the constituent material. Additional two points with a distance of approximately 100 μm from the interface were selected. In the PC case [Fig. 5(a)], where the materials are not mechanically coupled, the strain responses from locations close to the interface and further removed from the interface are almost identical. In contrast, the PSC case [Fig. 5(b)], featuring a mechanical interface, shows significant differences in the strain behavior when observing the composite close to the interface. Focusing on the remanent case, calculating the difference ($\Delta S = S_{1,0} - S_{1,x}$) between the average bulk strain $S_{1,0}$ and the strain S_{1x} at any chosen position x, one can infer the residual mechanical stress at this position. Doing so results in a positive value ($\Delta S = 0.007\%$) for the NBT–6BT layer, suggesting that the material contracted less at the interface than in the normalized case, resulting in tensile stress. On the other hand, negative values ($\Delta S = -0.012\%$) were calculated for the NBT–6BT–4KNN layer, suggesting a stronger contraction and, by extension, compressive stress. Assuming an isotropic, linear elastic response, the elastic moduli of the material can be used to estimate the value of the residual stress. For the calculations, an elastic modulus of approximately 105 GPa[58,59] for NBT–6BT and approximately 113 GPa[59] for NBT–6BT–4KNN, respectively, was chosen. It should be noted that the elastic modulus of NBT–6BT–4KNN was based on values reported for NBT–6BT–2KNN. Using these elastic properties, a residual stress close to the interface of approximately 10 MPa was estimated.

To further analyze the residual stress induced via the interface interaction, Figs. 6(a)–6(f) show the strain as a function of the position through the cross section of the composite structure with 20, 30, and 40 vol. % for both the PC and PSC cases. The same analysis can be found in a previous study for 50 vol. %.[45] In the unpoled state, there is no strain gradient through the thickness of either configuration. However, when an electric field is applied, a substantial increase in the strain gradient occurs. A sharp jump in strain is observed in the PC configuration when increasing the electric field over the respective poling field, as no mechanical connection is present between the two end members. The strain within each layer is uniform, although slight fluctuations as a function of position were apparent. This could be due to the aforementioned oil motion or an inhomogeneous electric field distribution inside the material.[60] Overall, no significant gradient or variation within the resolution of the current measurements is displayed. This is the case when increasing the electric field and when decreasing it. In contrast,

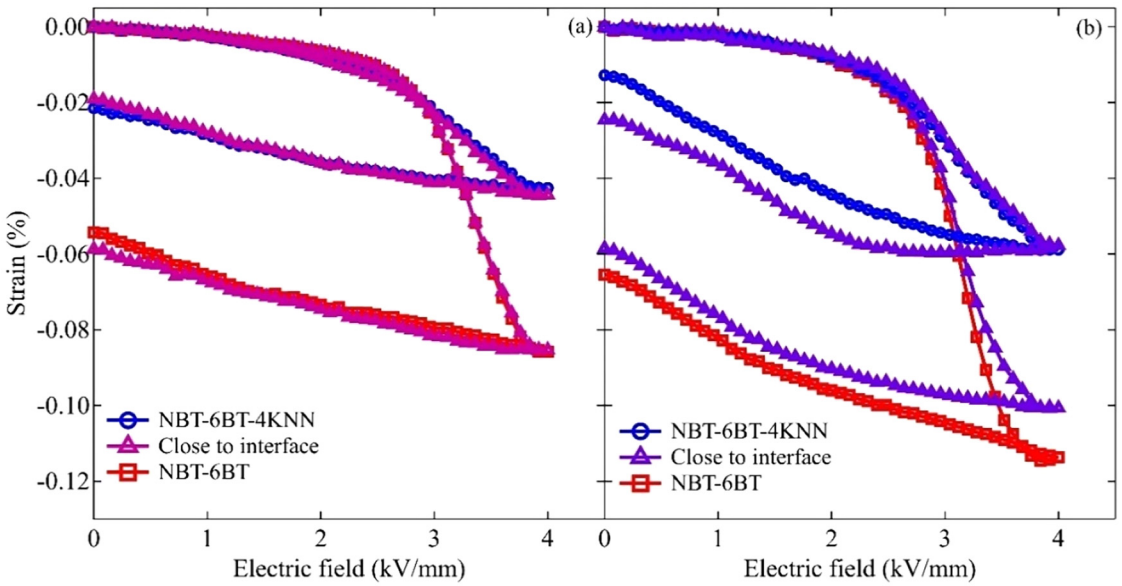

FIG. 5. Local transverse strain-electric field hysteresis loops at selected positions of the 2–2 composite with 40 vol. % NBT–6BT for the PC (a) and PSC case (b).

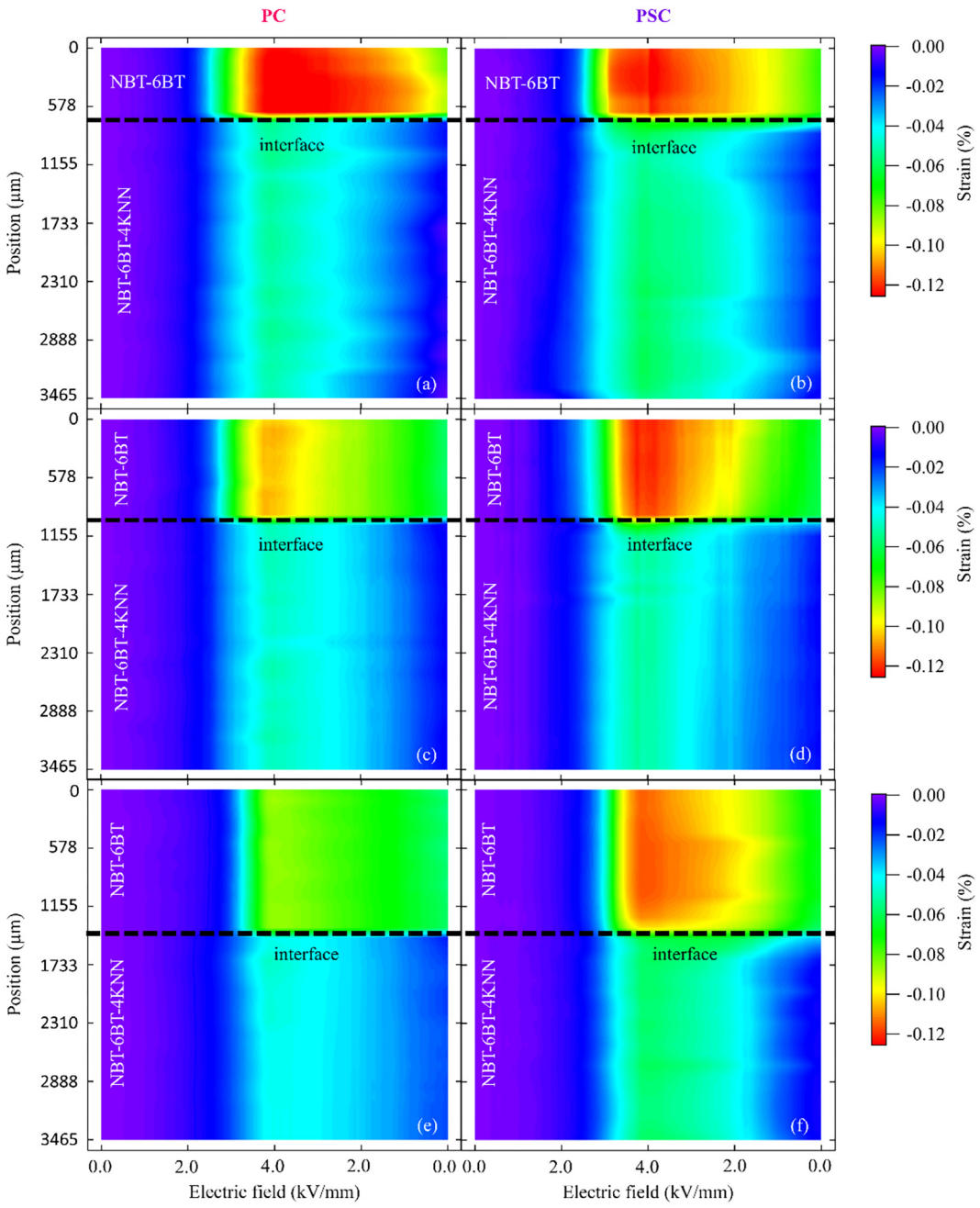

FIG. 6. Strain as a function of position and electric field for the PC and PSC case of 20 vol. % (a) and (b), 30 vol. % (c) and (d), and 40 vol. % (e) and (f). The black line indicates the interface between NBT–6BT and NBT–6BT–4KNN.

the mechanical interface in the PSC case resulted in a more gradual, continuous strain transition through the thickness of the composite structure. At the mechanical interface, the aforementioned tensile and compressive stresses are maximized for NBT–6BT and NBT–6BT–4KNN. Using the same method, a maximum residual stress of approximately 35 MPa was estimated for all vol. %. In particular, the compressive stress is essential for the observed enhancement of the electromechanical properties.[53,54] In a

previous study on PZT, a higher piezoelectric charge coefficient was achieved through radial compressive stress-assisted poling. It should be noted, however, that improved values were not observed after removal of the mechanical load. This, together with previous observations on bilayer composites,[45] suggests that a constant mechanical stress is crucial for the enhancement.

Nevertheless, the actual residual stress could be quite different, as a constant strain does not necessarily mean a stress-free region. For instance, the residual stress in each layer depends on the thickness ratio between the different layers. This is similar to residual stress generation during sintering of two materials with different sintering trajectories. This can be determined by the Chartier model,[61] which uses the classic laminate plate theory and describes the relationship between the tensile stresses in the NBT–6BT layer and the compressive stresses in the NBT–6BT–4KNN layer in the following equation:

$$\sigma_2 = -2\frac{t_1}{t_2}\,\sigma_1. \tag{2}$$

Here, t_1 and t_2 corresponds to the thickness of the NBT-6BT-4KNN and NBT-6BT layer, respectively. In general, this equation predicts that the compressive stress (σ_1) increases on the NBT-6BT-4KNN layer when its layer thickness becomes thinner compared to the layer thickness of NBT-6BT. In addition, the tensile stress (σ_2) on the NBT-6BT layer decreases. This change in ratio is equal to increasing the vol. % of NBT–6BT and should be reflected in the current observations. It should be noted that this equation was derived for trilayer composites, but the general relationship can be used to explain the observations of each vol. %. At a 20% volume fraction of NBT–6BT [Figs. 6(a) and 6(b)], the relatively thin layer of NBT–6BT, juxtaposed with the thicker layer of NBT–6BT–4KNN, resulted in pronounced tensile stress in NBT–6BT. While diminishing the strain response of NBT–6BT, the insufficient development of compressive stress limited the potential improvement in NBT–6BT–4KNN. This can be seen in the maximum strain in NBT–6BT, which did not reach the values compared to the PC case. As such, the thickness ratio of each layer is also the potential factor that resulted in the strain response of the

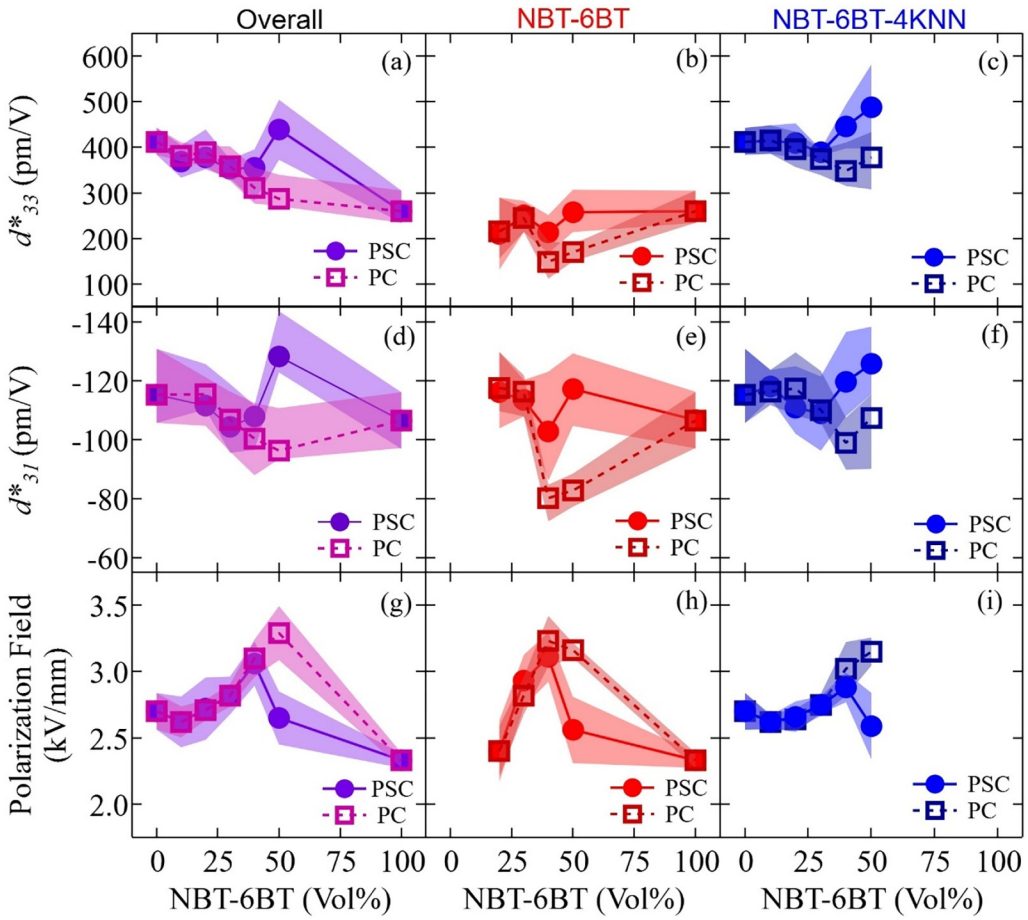

FIG. 7. Piezoelectric coefficients d^*_{33} (a)–(c), d^*_{31} (d)–(f), as well as polarization field (g)–(i) as a function of NBT–6BT content for the overall signal and both constituents. The shaded area represents the maximum and minimum measured values from six data points.

10 vol. % composites. Upon increasing the volume fraction to 30%, the thickness of NBT–6BT increased, leading to a reduction of the tensile stress in NBT–6BT, while increasing the compressive stress on NBT–6BT–4KNN. However, this increase did not translate into a significant enhancement in the performance of NBT–6BT–4KNN. In contrast, a 40% volume fraction of NBT–6BT proved to be a turning point. The increased thickness of NBT–6BT became sufficient to introduce beneficial compressive stress in NBT–6BT–4KNN. This configuration markedly improved overall properties, as the detrimental tensile stress in NBT–6BT was mitigated due to its increased thickness. As such, these observations emphasize the intricate relationship between volume fraction, layer thickness, and mechanical coupling in piezoelectric composites. The findings underscore the importance of considering these factors when optimizing the performance of such composite materials.

One of the important values for actuators is the large signal longitudinal piezoelectric coefficient d^*_{33}, which is determined by the difference in remanent and maximum unipolar strain normalized by the maximum applied electric field ($(S_{max} - S_{rem})/E_{max}$). Similarly, the large signal transverse piezoelectric coefficient d^*_{31} can be calculated by using the strain in the transverse direction, thus describing the contraction during the application of an electric field. These values, together with the polarization field, are summarized in Fig. 5; the total response in Figs. 7(a), 7(d), and 7(g), the NBT–6BT layer in Figs. 7(b), 7(e), and 7(h), and the NBT–6BT–4KNN layer in Figs. 7(c), 7(f), and 7(i). Additionally, the values for the PC and PSC cases are compared. For enhanced clarity, Fig. 7 presents the trend of the average value, with the shaded area denoting the range encompassing the maximum and minimum observed values. The overall signal shows, for the PC case, an almost linear decreasing trend from 410 pm/V to 260 pm/V with increasing seed concentration up to 50 vol. %, whereas an inverse behavior is seen for the polarization field. For seed contents between 0 and 20 vol. %, E_{pol} remains relatively constant at approximately 2.6 kV/mm. With increasing NBT–6BT content up to 50 vol. %, a value of 3.3 kV/mm is observed. The d^*_{31} values, on the other hand, remained relatively constant at approximately −110 pm/V, as NBT–6BT and NBT–6BT–4KNN displayed the same transverse strain response. If the end members are mechanically connected, however, the trend for all three values changes. At first, d^*_{33}, d^*_{31}, and E_{pol} follow the same behavior as the PC case, but diverge at 40 vol. %. The piezoelectric coefficients d^*_{33} and d^*_{31} are maximum at 50 vol. % with values of approximately 440 pm/V and −130 pm/V, respectively. Furthermore, the polarization field is significantly decreased at 50 vol. %, which is most likely caused by an increased local electric field. As the electrical contact was maintained, the polarization coupling did not change for the PSC case. The reason for the lower polarization field and improved electromechanical properties must, therefore, be a result of strain coupling.

The electromechanical response of NBT–6BT in the PC case shows a minimum at 40 to 50 vol. %, together with a maximum polarization field. Similar to the overall signal, strain coupling reduced the polarization field significantly. As such, d^*_{33} and d^*_{31} are improved compared to only polarization coupling. Nevertheless, the values are relatively constant for each volume fraction at approximately 220 pC/N and −110 pC/N for d^*_{33} and d^*_{31}, respectively. Thus, it is suggested that the overall improvement of the electromechanical properties stems more from the enhancement in the NBT–6BT–4KNN response. Here, d^*_{33} and d^*_{31} reach values at 50 vol. % of approximately 490 pm/V and −130 pm/V, respectively. For comparison, NBT–6BT–4KNN without an FE layer had values of 400 pm/V and −115 pm/V, thus enhancing these values by 25% and 15%, respectively. These results are similar to previous observations made by Groh *et al.*[39] where an optimized d^*_{33} was found for 50 vol. %. However, the observed composites were 0–3 composites and sintered together. It is most likely that interdiffusion and internal stresses also play a significant role in the changes to the electromechanical properties. Nevertheless, these results showed the importance of strain coupling for bilayer composites.

IV. CONCLUSION

Bilayer composites of NBT–6BT and NBT–6BT–4KNN were studied using digital image correlation, revealing the local strain response of each layer. The electromechanical properties were analyzed in both electrically connected (PC) and mechanically and electrically connected (PSC) cases. It was observed that strain coupling played a crucial role in enhancing the electromechanical response, especially in NBT–6BT–4KNN, where significant improvements in d^*_{33} and d^*_{31} of 25% and 15% compared to the pure end member, respectively, were observed at 50 vol. %. Interestingly, no significant differences were observed for cases between 10 and 30 vol. % for the bilayer materials. It is suggested that the thickness ratio played a pivotal role, and only at higher vol. % sufficient compressive stress was applied onto the NBT–6BT–4KNN layer. The stress-induced phase transformation through strain coupling led to an improved strain response, while polarization values were mostly consistent for the PC and PSC cases. These findings highlight the importance of strain coupling in bilayer composites and provide valuable insights for designing and optimizing lead-free piezoelectric materials for actuator applications.

SUPPLEMENTARY MATERIAL

See the supplementary material for SEM images of the microstructure and the grain size distribution of NBT–6BT and NBT–6BT–4KNN.

ACKNOWLEDGMENTS

A.M., J.M., and K.G.W. gratefully acknowledge the financial support of this work by the Deutsche Forschungsgemeinschaft (DFG) under Nos. WE4972/5 and GRK2495/F. In addition, this work was supported by the JSPS KAKENHI grant for Challenging Research (Grant No. 21K18821), the JSPS Japanese-German Graduate Externship (Grant No. 2019/R1), and an NITech grant for Young Researcher Projects 2021. A.M. would like to thank Dr. Di Chen for support with the DIC setup and Dr. Friedemann Streich for valuable discussions.

AUTHOR DECLARATIONS

Conflict of Interest

The authors have no conflicts to disclose.

Author Contributions

Alexander Martin: Conceptualization (equal); Data curation (lead); Formal analysis (lead); Investigation (equal); Methodology (equal); Software (equal); Validation (equal); Visualization (lead); Writing – original draft (lead). **Juliana G. Maier:** Formal analysis (supporting); Investigation (equal); Methodology (equal); Validation (equal); Writing – review & editing (equal). **Ken-ichi Kakimoto:** Resources (supporting); Supervision (supporting); Writing – review & editing (equal). **Marc Kamlah:** Conceptualization (equal); Funding acquisition (equal); Project administration (equal); Resources (supporting); Supervision (supporting); Validation (equal); Writing – review & editing (equal). **Kyle G. Webber:** Conceptualization (equal); Funding acquisition (equal); Methodology (equal); Project administration (equal); Resources (lead); Supervision (lead); Writing – review & editing (equal).

DATA AVAILABILITY

The data that support the findings of this study are available from the corresponding author upon reasonable request.

REFERENCES

[1]P. Fan, K. Liu, W. Ma, H. Tan, Q. Zhang, L. Zhang, C. Zhou, D. Salamon, S. T. Zhang, Y. Zhang, B. Nan, and H. Zhang, J. Mater. **7**, 508 (2021).
[2]J. Rödel, K. G. Webber, R. Dittmer, W. Jo, M. Kimura, and D. Damjanovic, J. Eur. Ceram. Soc. **35**, 1659–1681 (2015).
[3]P. K. Panda, B. Sahoo, T. S. Thejas, and M. Krishna, J. Electron. Mater. **51**, 938–952 (2022).
[4]S.-T. Zhang, A. B. Kounga, E. Aulbach, H. Ehrenberg, and J. Rödel, Appl. Phys. Lett. **91**, 112906 (2007).
[5]J. Wu, H. Zhang, C.-H. Huang, C.-W. Tseng, N. Meng, V. Koval, Y.-C. Chou, Z. Zhang, and H. Yan, Nano Energy **76**, 105037 (2020).
[6]W. Jo, R. Dittmer, M. Acosta, J. Zang, C. Groh, E. Sapper, K. Wang, and J. Rödel, J. Electroceram. **29**, 71–93 (2012).
[7]H. Zhang, W. Ma, B. Xie, L. Zhang, S. Dong, P. Fan, K. Wang, J. Koruza, and J. Rödel, J. Am. Ceram. Soc. **102**, 6147–6155 (2019).
[8]S. Gorfman and P. A. Thomas, J. Appl. Crystallogr. **43**, 1409–1414 (2010).
[9]E. Aksel, J. S. Forrester, J. L. Jones, P. A. Thomas, K. Page, and M. R. Suchomel, Appl. Phys. Lett. **98**, 152901 (2011).
[10]S. B. Vakhrushev, V. A. Isupov, B. E. Kvyatkovsky, N. M. Okuneva, I. P. Pronin, G. A. Smolensky, P. P. Syrnikov, and A. F. Ioffe, Ferroelectrics **63**, 153–160 (1985).
[11]G. O. Jones and P. A. Thomas, Acta Crystallogr. B: Struct. Sci. **58**, 168–178 (2002).
[12]B. N. Rao, A. N. Fitch, and R. Ranjan, Phys. Rev. B **87**, 060102 (2013).
[13]V. Dorcet, G. Trolliard, and P. Boullay, J. Magn. Magn. Mater. **321**, 1758–1761 (2009).
[14]R. Beanland and P. A. Thomas, Scr. Mater. **65**, 440–443 (2011).
[15]F. Li, S. Zhang, D. Damjanovic, L.-Q. Chen, and T. R. Shrout, Adv. Funct. Mater. **28**, 1801504 (2018).
[16]T. Zheng, J. Wu, D. Xiao, and J. Zhu, Prog. Mater. Sci. **98**, 552–624 (2018).
[17]K. Riess, N. H. Khansur, A. Martin, A. Benčan, H. Uršič, and K. G. Webber, Phys. Rev. B **103**, 94113 (2021).
[18]K. Yoshii, Y. Hiruma, H. Nagata, and T. Takenaka, Jpn. J. Appl. Phys. **45**, 4493 (2006).
[19]Y. Ehara, N. Novak, A. Ayrikyan, P. T. Geiger, and K. G. Webber, J. Appl. Phys. **120**, 174103 (2016).
[20]M. Acosta, W. Jo, and J. Rödel, J. Am. Ceram. Soc. **97**, 1937–1943 (2014).
[21]W. P. Cao, J. Sheng, Y. L. Qiao, L. Jing, Z. Liu, J. Wang, and W. L. Li, J. Eur. Ceram. Soc. **39**, 4046–4052 (2019).
[22]T. Takenaka, K. Maruyama, and K. Sakata, Jpn. J. Appl. Phys. **30**, 2236 (1991).
[23]G. Picht, J. Töpfer, and E. Hennig, J. Eur. Ceram. Soc. **30**, 3445–3453 (2010).
[24]C. Ma, H. Guo, S. P. Beckman, and X. Tan, Phys. Rev. Lett. **109**, 107602 (2012).
[25]A. Martin, N. H. Khansur, and K. G. Webber, J. Eur. Ceram. Soc. **38**, 4623–4630 (2018).
[26]C. Xu, D. Lin, and K. W. Kwok, Solid State Sci. **10**, 934–940 (2008).
[27]F. Craciun, C. Galassi, and R. Birjega, J. Appl. Phys. **112**, 124106 (2012).
[28]V. Bobnar, Z. Kutnjak, R. Pirc, and A. Levstik, Phys. Rev. B **60**, 6420–6427 (1999).
[29]C. A. Randall, D. J. Barber, and R. W. Whatmore, J. Microsc. **145**, 275 (1987).
[30]R. Sommer, N. K. Yushin, and J. J. Van Der Klink, Phys. Rev. B **48**, 13230–13237 (1993).
[31]N. H. Khansur, U. Eckstein, H. Ursic, M. Sadl, M. Brehl, A. Martin, K. Riess, D. de Ligny, and K. G. Webber, Adv. Mater. Interfaces **8**, 2100309 (2021).
[32]W. Jo, T. Granzow, E. Aulbach, J. Rödel, and D. Damjanovic, J. Appl. Phys. **105**, 094102 (2009).
[33]C. W. Ahn, C.-H. Hong, B.-Y. Choi, H.-P. Kim, H.-S. Han, Y. Hwang, W. Jo, K. Wang, J.-F. Li, J.-S. Lee, and I. W. Kim, J. Korean Phys. Soc. **68**, 1481–1494 (2016).
[34]D. S. Lee, D. H. Lim, M. S. Kim, K. H. Kim, and S. J. Jeong, Appl. Phys. Lett. **99**, 062906 (2011).
[35]D. Su Lee, S. Jong Jeong, M. Soo Kim, and J. Hyuk Koh, J. Appl. Phys. **112**, 124109 (2012).
[36]D. E. Dausch, E. Furman, F. Wang, and G. H. Haertling, Ferroelectrics **177**, 221–236 (1996).
[37]D. E. Dausch, E. Furman, F. Wang, and G. H. Haertling, Ferroelectrics **177**, 237–253 (1996).
[38]C. Groh, D. J. Franzbach, W. Jo, K. G. Webber, J. Kling, L. A. Schmitt, H.-J. Kleebe, S.-J. Jeong, J.-S. Lee, and J. Rödel, Adv. Funct. Mater. **24**, 356–362 (2014).
[39]C. Groh, W. Jo, and J. Rödel, J. Am. Ceram. Soc. **97**, 1465–1470 (2014).
[40]P. Fan, Y. Zhang, Y. Zhu, W. Ma, K. Liu, X. He, M. A. Marwat, B. Xie, M. Li, and H. Zhang, J. Am. Ceram. Soc. **102**, 4113–4126 (2019).
[41]H. Zhang, C. Groh, Q. Zhang, W. Jo, K. G. Webber, and J. Rödel, Adv. Electron. Mater. **1**, 1500018 (2015).
[42]A. Ayrikyan, V. Rojas, L. Molina-luna, M. Acosta, J. Koruza, and K. G. Webber, IEEE Trans. Ultrason. Ferroelectr. Freq. Control **62**, 997–1006 (2015).
[43]A. Ayrikyan, F. Weyland, S. Steiner, M. Duerrschnabel, L. Molina-Luna, J. Koruza, and K. G. Webber, J. Am. Ceram. Soc. **100**, 3673–3683 (2017).
[44]A. Ayrikyan, O. Prach, N. H. Khansur, S. Keller, S. Yasui, M. Itoh, O. Sakata, K. Durst, and K. G. Webber, Acta Mater. **148**, 432–441 (2018).
[45]A. Martin, J. G. Maier, F. Streich, M. Kamlah, and K. G. Webber, Smart Mater. Struct. **31**, 075009 (2022).
[46]M. Saleem, L. D. Hwan, I. sung Kim, M. S. Kim, A. Maqbool, U. Nisar, S. A. Pervez, U. Farooq, M. U. Farooq, H. M. W. Khalil, and S. J. Jeong, Sci. Rep. **8**, 14146 (2018).
[47]R. Dittmer, W. Jo, J. Rödel, S. Kalinin, and N. Balke, Adv. Funct. Mater. **22**, 4208–4215 (2012).
[48]S.-T. Zhang, A. B. Kounga, E. Aulbach, T. Granzow, W. Jo, H.-J. Kleebe, and J. Rödel, J. Appl. Phys. **103**, 034107 (2008).
[49]C. S. Lynch, Acta Mater. **44**, 4137–4148 (1996).
[50]X. Tan, J. Frederick, C. Ma, E. Aulbach, M. Marsilius, W. Hong, T. Granzow, W. Jo, and J. Rödel, Phys. Rev. B **81**, 014103 (2010).
[51]S. Takasaka, Y. Tsujimi, and T. Yagi, Phys. Rev. B **65**, 174102 (2002).
[52]W. Jo and J. Rödel, Appl. Phys. Lett. **99**, 042901 (2011).
[53]T. Granzow, T. Leist, A. B. Kounga, E. Aulbach, and J. Rödel, Appl. Phys. Lett. **91**, 142904 (2007).
[54]A. Kounga Njiwa, E. Aulbach, T. Granzow, and J. Rödel, Acta Mater. **55**, 675–680 (2007).
[55]X. Tan, E. Aulbach, W. Jo, T. Granzow, J. Kling, M. Marsilius, H.-J. Kleebe, and J. Rodel, J. Appl. Phys. **106**, 44107 (2009).

[56]R. Dittmer, K. G. Webber, E. Aulbach, W. Jo, X. Tan, and J. Rödel, Acta Mater. **61**, 1350–1358 (2013).
[57]F.-C. Sun, M. T. Kesim, Y. Espinal, and S. P. Alpay, J. Mater. Sci. **51**, 499–505 (2016).
[58]M. Vögler, N. Novak, F. H. Schader, and J. Rödel, Phys. Rev. B **95**, 024104 (2017).
[59]R. Dittmer, W. Jo, K. G. Webber, J. L. Jones, and J. Rödel, J. Appl. Phys. **115**, 084108 (2014).
[60]Z. Liu, X. Fan, K. Liu, F. Zhang, B. Huang, Y. Wang, and J. Li, Appl. Phys. Lett. **123**, 162901 (2023).
[61]T. Chartier, D. Merle, and J. L. Besson, J. Eur. Ceram. Soc. **15**, 101–107 (1995).